AIAA Aviation Forum and ASCEND co-located Conference Proceedings
21 - 25 July 2025, Las Vegas, Nevada
AIAA AVIATION FORUM AND ASCEND 2025

10.2514/6.2025-3703

Study of 2D Hover Performance Using Flapped Coflow Jet Airfoil at Low Reynolds Numbers

Jaehyoung Jeon * Anthony Diaz † Yan Ren ‡ Gecheng Zha §
Dept. of Mechanical and Aerospace Engineering
University of Miami, Coral Gables, Florida 33124
E-mail: gzha@miami.edu

Abstract

This paper conducts a trade study of a deflected slipstream system utilizing flapped coflow jet (FCFJ) airfoils for achieving optimal hover performance for fixed wing VTOL aircraft at low Reynolds number conditions in the Martian atmosphere. The deflected slipstream configuration is advantageous for vertical takeoff and landing because it avoids tilting rotors, wings, or using lift-plus-cruise configurations while enabling efficient runway-independent operations. The objective is to find the optimal FCFJ airfoil configuration that generates the required hover lift with minimal coflow jet and propeller power at low Reynolds numbers. The in-house validated 2D URANS solver with Spalart-Allmaras (SA) turbulence model, a third-order WENO scheme for inviscid fluxes, and second-order central differencing for viscous terms are used for the computational fluid dynamics simulations. The parametric study reveals a highly fairly linear relationship between propeller strength D_p and total lift coefficient, with CFJ injection size exhibiting an inverse power-law scaling with total pressure ratio following $\Gamma \propto \text{Inj\_size}(\%C)^{-0.4}$. Results indicate that achieving the target lift coefficient of 72 initially requires excessively large injection slots (3.2%C) and high momentum coefficients C_μ of 30. However, a aircraft system tilting of 20deg with flap deflection $\beta = 60$ successfully achieves the target performance while reducing CFJ power coefficient by 65% and utilizing feasible injection and suction slot dimensions of 0.6%C and 1.3%C, respectively. The final configuration demonstrates that flow attachment is maintained at $C_\mu \geq 3$, providing critical design guidelines for efficient VTOL operations in the thin Martian atmosphere.

Nomenclature

CFJ	CoFlow jet
$FCFJ$	Flapped CoFlow jet
A	Propeller disk area
$AoA(\alpha)$	Angle of attack
LE	Leading Edge

* Ph.D. Candidate
† Master Student
‡ Postdoc Researcher, Ph.D., AIAA member
§ Professor, ASME Fellow, AIAA associate Fellow

TE	Trailing Edge
C_L	Lift coefficient $L/(q_\infty S)$
C_D	Drag coefficient $D/(q_\infty S)$
C_μ	Jet momentum coef. $\dot{m}_j U_j/(q_\infty S)$
$(C_L/C_D)_c$	CFJ airfoil corrected aerodynamic efficiency $C_L/(C_D$+Pc)
$(C_L^2/C_D)_c$	CFJ airfoil corrected productivity efficiency $C_L^2/(C_D$+Pc)
D	Propeller Diameter
DS	Deflected Slipstream
DL	Disk loading, thrust of actuator disk/actuator disk area
DL_c	Disk loading coefficient
FM_{DS}	Figure of Merit for the DS system
P_{tot}	Total power of the DS-CFJ system
P_P	Propeller actuator power coefficient $\frac{2}{\rho V_\infty^3 S}\sqrt{\frac{F^3}{2\rho A}}$
PL	Power loading, power/lift
PL_c	Power loading coefficient
D_p	Pressure percentage increase across the propeller actuator disk (ΔP)
R	Propeller disk radius
R_e	Reynolds number
M	Mach number
S	Planform area of the wing
T_t	Total temperature
P_t	Total pressure
H_t	Total specific enthalpy
U	Flow velocity
P	Pumping power
P_c	Power coefficient $P/(q_\infty S V_\infty)$
c_p	Constant pressure specific heat
γ	Air specific heats ratio
s	Wing Span length
c	Profile chord
q	Dynamic pressure $0.5\,\rho U^2$
p	Static pressure
ρ	Air density
β	Deflection angle
$\dot{m}$	Mass flow across the pump
ϵ	Resultant force angle
Γ	Total pressure ratio of compressor
θ	airfoil tilting angle
$_\infty$	Subscript, stands for free stream
$_j$	Subscript, stands for jet

1 Introduction

Mars exploration demands technological advancements to enlarge operational range of aerial vehicles on the Martian surface. Mars' unique environment presents significant challenges for aerial mobility due

to its thin atmosphere and varied terrain. High-performance, efficient aircraft specifically designed for Mars are essential for future missions to enhance mobility and accessibility, facilitating exploration of vast Martian landscapes, resource discovery, water and ice deposit identification, methane source detection, and insights into Martian geological history.

One of the primary challenges in developing aircraft for Mars is achieving ultra-high lift coefficients to minimize vehicle size and weight in the thin Martian atmosphere, which is characterized by low Reynolds numbers and low air density. With an atmospheric density roughly 1% that of Earth's, Mars requires innovative aerodynamic solutions, as traditional Earth-based aircraft designs relying on standard airfoil interactions for lift are not feasible. This distinct atmospheric characteristic demands a paradigm shift in aerodynamic design to achieve sustained flight performance on Mars [1].

Vertical takeoff and landing (VTOL) technology has emerged as a key area of interest due to its unique capability for runway-independent operations. In terrestrial applications, urban air mobility is accelerating demand for advanced VTOL technologies, particularly for electric vertical takeoff and landing (eVTOL) aircraft [2], which play a critical role in the evolution of urban transportation and e-commerce logistics. Current first-generation eVTOL technology primarily relies on traditional rotorcraft principles, employing vertical propellers for hovering, as seen in tiltrotor (e.g., V-280, V-22, Joby), tiltwing (e.g., Hiller X-18, Airbus Vahana), and lift-plus-cruise (e.g., SB-1, Wisk) configurations. These designs have advantages over conventional rotorcraft by utilizing distributed propulsion with multiple small propellers, which reduces noise, enhances efficiency, and enables higher cruise speeds in conjunction with fixed-wing configurations.

While conventional rotorcraft achieve efficient hovering by exhausting flow downward (downwash) using vertical propellers, they encounter limitations in forward flight. Specifically, three primary challenges exist: 1) Complexity: Tiltrotors and tiltwings require intricate mechanical systems to reorient propellers for forward flight, leading to higher weight and potential reliability concerns. Additionally, transition phases between hover and cruise present challenges in achieving stable lift and balance at intermediate speeds. 2) Noise: Rotorcraft generate significant broadband noise during hovering due to flow separation and turbulent wake interactions between the rotor downwash and the airfoil, which is difficult to mitigate. 3) Range: VTOL vehicles based on rotorcraft designs generally have lower mission efficiency and range due to added weight and drag from components used solely for hovering, such as dedicated lift propellers, struts, and tilting mechanisms.

The objective of this paper is to optimize deflected slipstream (DS) technology [2, 3, 4] to enhance VTOL hover efficiency without relying on conventional tilting rotors, tilting airfoils, or lift-plus-cruise configurations. However, the aerodynamic efficiency drops significantly at low Reynolds number that can significantly affect the system efficiency and effectiveness. The purpose of this paper is to investigate the optimal deflected slipstream configuration that enables efficient low Reynolds number operations for runway-independent environments such as Mars.

1.1 CoFlow Jet (CFJ) Active Flow Control

Active flow control (AFC) has emerged as a promising technology to improve aerodynamic performance, particularly for increasing maximum lift coefficient (C_{Lmax}) by suppressing flow separation and enhancing airfoil circulation. This is achieved by adding energy to the flow, typically through techniques such as blowing or suction. However, integrating AFC for cruise operation presents a significant challenge. While the benefits of increased C_{Lmax} are evident, they need to outweigh the energy consumption associated

with the AFC system itself for the overall aircraft to achieve a net efficiency gain. One promising AFC technology with the potential to overcome this challenge and enhance cruise efficiency is the CoFlow Jet (CFJ) flow control airfoil[5, 6, 7, 8, 9, 10, 11, 12, 13, 14, 15, 16, 17, 18, 19, 20]. This innovative design utilizes a series of small, jet-powered actuators embedded within the airfoil's surface. These actuators inject a high-momentum fluid stream parallel to the main airflow, which effectively energizes the boundary layer and delays flow separation. For a regular CFJ airfoil, as shown in Fig. 1, a small amount of mass flow is drawn into the suction duct, pressurized and powered by a pump, and then injected near the LE tangentially to the main flow. In comparison with the 2D baseline airfoil, Wang and Zha[21] show that the 2D CFJ airfoil can achieve a significantly higher cruise lift coefficient and aerodynamic efficiency, defined as

$$(\frac{C_L}{C_D})_c = \frac{C_L}{C_D + P_c} \tag{1}$$

While CoFlow Jet (CFJ) technology offers promising avenues for enhancing cruise performance, it is crucial to evaluate its impact on overall aircraft efficiency. This necessitates consideration of the CFJ power requirement, denoted by the CFJ required power coefficient, Pc. Studies have shown that CFJ wings can maintain high cruise lift coefficient(C_L) even for three-dimensional wings with finite aspect ratios. However, this improved lift performance comes at the cost of reduced aerodynamic efficiency, which can potentially decrease to the level of conventional baseline wings, as reported by Wang et al. [22]. To comprehensively assess the transportation productivity of aircraft, a parameter encompassing both range and gross weight is introduced: cruise productivity efficiency. This metric, proposed by Yang et al. [16], provides a more holistic evaluation of aircraft performance, considering not just aerodynamic efficiency but also payload capacity and range capability.

$$(\frac{C_L^2}{C_D})_c = \frac{C_L^2}{(C_D + Pc)} \tag{2}$$

A CFJ wing can have substantially higher cruise C_L and thus greater productivity efficiency as well. Taking advantage of the CFJ wing high cruise lift coefficient and thus high suction effect on the wing's upper surface, Ren and Zha [23] design a tandem wing aircraft configuration that the front wing tip vortex is captured by the rear wing to enhance the overall system efficiency. However, for cruise condition, the regular CFJ configuration as shown in Fig. 1 appears to have rapid energy consumption increase when C_L is greater than 1.6[16, 24]. Even though the aerodynamic drag coefficient C_D can remain small and the pure aerodynamic lift-to-drag ratio C_L/C_D can still be very high, the corrected aerodynamic efficiency defined in Eq. (1) can decrease quickly with the increasing C_L.

Flapped CoFlow Jet technology has emerged as a promising solution for achieving high C_L while maintaining acceptable $(C_L/C_D)_c$. This capability makes it particularly relevant for aircraft operating in low-density environments, such as at high altitudes on Earth or in the Martian atmosphere. As demonstrated in previous studies[25, 26, 27, 28], flapped CFJs can significantly enhance lift performance, opening opportunities for various mission applications. Based on these studies, we will investigate whether the use of a very large deflection angle beta can result in a defelected slipstream flow and enable flight in vertical takeoff, landing, and hover conditions.

1.2 Flapped CoFlow Jet Airfoil

The concept of flapped coflow jet airfoil is adopted from the CFJ airfoil with deflected slipstream for VTOL aircraft [4]. It is also guided by the CoFlow jet flow separation mechanism study of Xu and Zha [29].

The CFJ is applied inside a long flap that is a part of the flapped CFJ airfoil, as shown in Fig.1 [25], which has the injection located at the shoulder of the flap. The regular CFJ airfoil applies the injection very close to the leading edge at a point of around 2-4% Chord location. By deflecting the flap rather than rotating the front of the airfoil, the FCFJ airfoil has the advantage of allowing the airfoil to change the angle of attack and lift coefficient without tilting the wings or the aircraft. The purpose of this paper is to numerically demonstrate that the coflow jet is feasible to deflect the slipstream of a propeller by an airfoil with a simple plain flap at low energy expenditure. This will lay a foundation for further development of the DS-CFJ technology at low Reynolds number.

Figure 2 schematizes the geometric configuration and force vector relationships for a flapped coflow jet (FCFJ) airfoil system. The propellers are mounted vertically above the airfoil, positioned at a specified distance from the leading edge to optimize slipstream interaction. The entire system can be tilted collectively by an angle (θ) degrees from the horizontal reference plane, providing additional control for hover performance optimization.

The epsilon angle (ϵ) represents the resultant force direction relative to the vertical axis, serving as a key performance indicator for deflected slipstream effectiveness. When epsilon equals 90 degrees, the resultant force is perfectly vertical, indicating optimal hover configuration. If epsilon is smaller than 90 degrees, the resultant force has a drag component pointing downstream, while epsilon greater than 90 degrees creates a thrust component directed upstream.

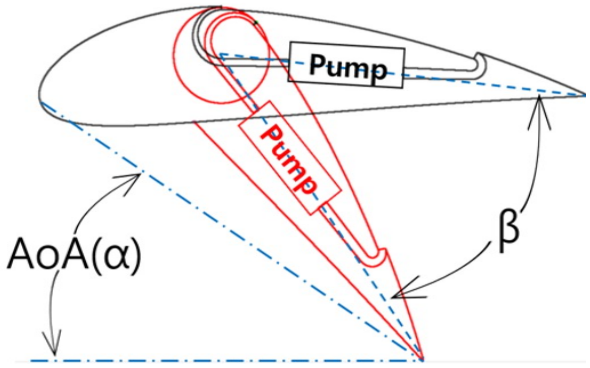

Figure 1: Sketch of flapped CFJ airfoil with the CoFlow jet applied on the flap

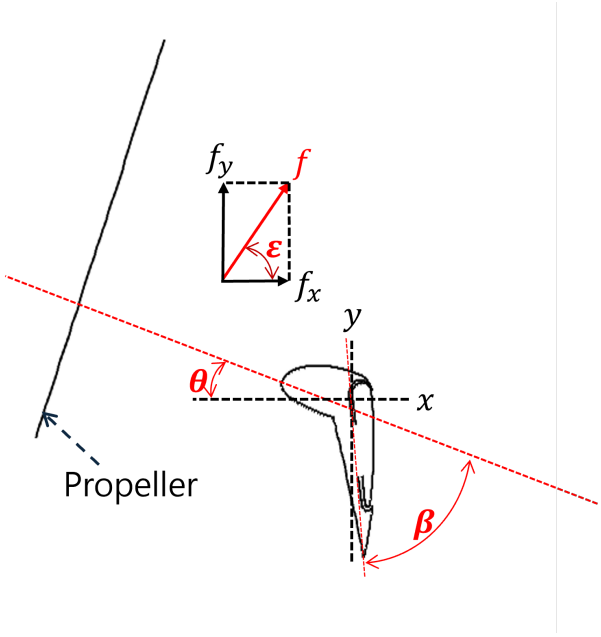

Figure 2: schematic of the geometric configuration and resultant force

2 Methodology

2.1 Lift and Drag Calculation

The momentum and pressure at the injection and suction slots produce a reactionary force, which is automatically measured by the force balance in wind tunnel testing. However, for CFD simulation, the full reactionary force needs to be included. Using control volume analysis, the reactionary force can be calculated using the flow parameters at the injection and suction slot opening surfaces. Zha et al. [6] give the following formulations to calculate the lift and drag due to the jet reactionary force for a CFJ airfoil. By considering the effects of injection and suction jets on the CFJ airfoil, the expressions for these reactionary forces are given as :

$$F_{x_{cfj}} = (\dot{m}_j V_{j1} + p_{j1} A_{j1}) * cos(\theta_1 - \alpha) - (\dot{m}_j V_{j2} + p_{j2} A_{j2}) * cos(\theta_2 + \alpha) \tag{3}$$

$$F_{y_{cfj}} = (\dot{m}_{j1} V_{j1} + p_{j1} A_{j1}) * sin(\theta_1 - \alpha) + (\dot{m}_{j2} V_{j2} + p_{j2} A_{j2}) * sin(\theta_2 + \alpha) \tag{4}$$

where the subscripts 1 and 2 stand for the injection and suction respectively, and θ_1 and θ_2 are the angles between the injection and suction slot's surface and a line normal to the airfoil chord. α is the angle of attack.

The total lift and drag on the airfoil can then be expressed as:

$$D = R'_x - F_{x_{cfj}} \tag{5}$$

$$L = R'_y - F_{y_{cfj}} \tag{6}$$

where R'_x and R'_y are the surface integral of pressure and shear stress in x (drag) and y (lift) direction excluding the internal ducts of injection and suction. For CFJ wing simulations, the total lift and drag are calculated by integrating Eqs.(5) and (6) in the spanwise direction.

2.2 Jet Momentum Coefficient

The jet momentum coefficient C_μ is a parameter used to quantify the jet intensity. It is defined as:

$$C_\mu = \frac{\dot{m} V_j}{\frac{1}{2} \rho_\infty {V_\infty}^2 S} \tag{7}$$

where $\dot{m}$ is the injection mass flow, V_j is the mass-averaged injection velocity, ρ_∞ and V_∞ denote the free stream density and velocity, and S is the planform area.

2.3 Micro-compressor Power Coefficient

CFJ is implemented by mounting a pumping system inside the wing that withdraws air from the suction slot and blows it into the injection slot. The power consumption is determined by the jet mass flow and total enthalpy change as the following:

$$P = \dot{m}(H_{t1} - H_{t2}) \tag{8}$$

where H_{t1} and H_{t2} are the mass-averaged total enthalpy in the injection cavity and suction cavity respectively, P is the Power required by the pump and $\dot{m}$ the jet mass flow rate. Introducing P_{t1} and P_{t2} the mass-averaged total pressure in the injection and suction cavity respectively, the compressor efficiency η, and the total pressure ratio of the pump $\Gamma = \frac{P_{t1}}{P_{t2}}$, the power consumption is expressed as:

$$P = \frac{\dot{m}C_pT_{t2}}{\eta}(\Gamma^{\frac{\gamma-1}{\gamma}} - 1) \tag{9}$$

where γ is the specific heat ratio equal to 1.4 for air. The power coefficient is expressed as:

$$P_c = \frac{P}{\frac{1}{2}\rho_\infty V_\infty^3 S} \tag{10}$$

2.4 Aerodynamic Efficiency

The conventional wing aerodynamic efficiency is defined as:

$$\frac{C_L}{C_D} \tag{11}$$

For the CFJ wing, the ratio above still represents the pure aerodynamic relationship between lift coefficient and drag coefficient. However since CFJ active flow control consumes energy, the ratio above is modified to take into account the energy consumption of the micro-compressor. The formulation of the corrected aerodynamic efficiency for CFJ wings is:

$$(\frac{C_L}{C_D})_c = \frac{C_L}{C_D + P_c} \tag{12}$$

where P_c is the micro-compressor power coefficient defined in Eqn. 10 and C_L and C_D are the lift and drag coefficients of the CFJ wing. If the micro-compressor power coefficient is set to 0, this formulation returns to the aerodynamic efficiency of a conventional airfoil.

2.5 Disk Loading and Power Loading

For rotorcraft aerodynamics, the ideal power coefficient for the propeller-based actuator disk momentum theory at static condition is:

$$P_p = \frac{2}{\rho_\infty V_\infty^3 S}\sqrt{\frac{L^3}{2\rho A}} \tag{13}$$

where A is the actuator disk area; L is the total force produced by the propeller actuator normal to the propeller disk. L would be the lift for a vertical rotor or thrust for a horizontal rotor. The same reference parameters for the airframe aerodynamic parameters are used to normalize the rotor parameters to be consistent.

Disk loading and power loading are used to describe rotorcraft VTOL performance. The disk loading (DL) is defined as

$$DL = \frac{L}{A} \tag{14}$$

The disk loading is closely related to the noise produced by a rotor. A higher disk loading will in general generate louder noise. The power loading (PL) for a propeller disk at static hovering condition is defined as

$$PL = \frac{P}{L} \tag{15}$$

where P is the propeller power used to generate the lift L. The power loading indicates the power required per unit lift for rotorcraft. The disk loading and power loading coefficients are defined as follows:

$$DL_c = \frac{DL}{0.5\rho_\infty V_\infty^2} = \frac{C_L}{A_c} \tag{16}$$

where $C_L = L/(0.5\rho V^2 S)$, $A_c = A/S$, A is the disk area and S is the wing planform area.

$$PL_c = \frac{PL}{V_\infty} = \frac{P_p}{C_L} \tag{17}$$

The actuator DL and PL have the following relations in hover static condition:

$$PL = \sqrt{\frac{DL}{2\rho}} \tag{18}$$

$$PL_c = \frac{\sqrt{DL_c}}{2} \tag{19}$$

2.6 Figure of Merit for DS-CFJ Hover

To compare the efficiency of the DS-CFJ hover system with a vertical rotor with the same total lift and disk size, we adopt a parameter FM_{DS} similar to the figure of merit (FM) of rotorcraft below:

$$FM_{DS} = \frac{P_p}{P_{DS-CFJ}} = \frac{P_p}{P_{prop} + P_c} \tag{20}$$

where P_p is the ideal power coefficient required by a vertical rotor disk that generates the same lift of the DS-CFJ system with the same rotor disk size based on Eq. 13. The total power required by the DS-CFJ system P_{DS-CFJ} is the summation of the propeller power P_{prop} and the CFJ power P_c.

To isolate the CFJ effect in the parameter FM_{DS}, the propeller power P_{prop} of the DS-CFJ system is also calculated based on the disk theory formulation Eq. 13, which uses the disk loading determined by the pressure rise imposed on the disk as the boundary condition. The CFJ power required P_c is determined by Eq. 9 and 10. The power coefficient P_c studied in this paper includes all the viscous effect of the DS-CFJ system governed by Reynolds averaged Navier-Stokes (RANS) equations, but the CFJ actuator efficiency in Eq. 9 is set to be 100% to consider only the power required to achieve the AFC performance. Currently, the efficiency of a micro-compressor with the diameter of 64 mm we have designed is slightly more than 84% [30]. In an integrated system with a CFJ airfoil and a micro-compressor actuator, the micro-compressor efficiency is designed to 76%-80% [31, 32]. Such efficiency corresponds to a typical figure of merit of vertical rotors. With more design optimization, a higher micro-compressor efficiency is achievable. If FM_{DS} is larger than one, the DS-CFJ system has the same hover efficiency as a vertical rotor with the same rotor disk size.

2.7 CFD Simulation Setup

The FASIP(Flow-Acoustics-Structure Interaction Package) CFD code is used to conduct the numerical simulation. The 2D unsteady Reynolds Averaged Navier-Stokes (URANS) equations with one-equation Spalart-Allmaras(SA) turbulence model is used. A 3rd order WENO scheme for the inviscid flux [33, 34, 35, 36, 37, 38] and a 2nd order central differencing for the viscous terms [33, 37] are employed to discretize the Navier-Stokes equations. The low diffusion E-CUSP scheme used as the approximate Riemann solver suggested by Zha et al [34] is utilized with the WENO scheme to evaluate the inviscid fluxes. Implicit time marching method using Gauss-Seidel line relaxation is used to achieve a fast convergence rate [39]. Parallel computing is implemented to save wall clock simulation time [40].

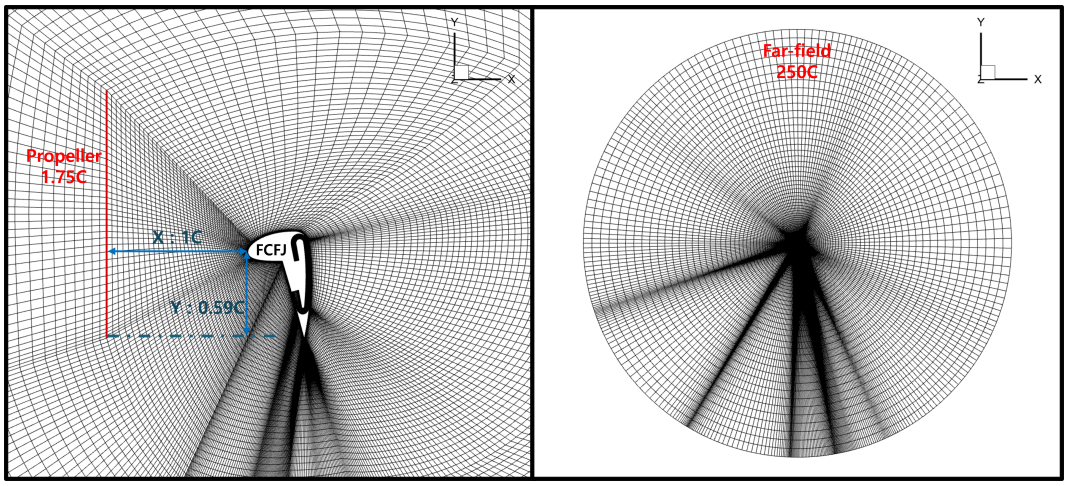

Figure 3: 2D mesh for the hover condition.

2.8 Boundary Conditions

The 3rd order accuracy no slip condition is enforced on the solid surface with the wall treatment suggested in [41] to achieve the flux conservation on the wall. The far field boundary is located at 250 chord with an O-mesh topology. The computational mesh is shown in Fig. 3. Total pressure, total temperature and flow angles are specified at the injection duct inlet, as well as the upstream portion of the far field. For the static condition, the static pressure at the downstream farfield is set to be equal to the total pressure at upstream far field. Constant static pressure is applied at the suction duct outlet as well as the downstream portion of the far field. The domain size is about 500 chords away from the airfoil to ensure solid convergence at the static flow conditions.

The actuator disk BC is modeled as a flat surface, across which the static pressure is increased by a percentage ΔP based on the local static pressure upstream of the disk. Even though the pressure increase percentage is uniform across the disk, the pressure increase is not uniform due to the non-uniform local static pressure upstream of the disk. The pressure jump across the disk is handled by the approximate Riemann solver in the FASIP code similar to a shock wave.

To avoid being divided by zero, the freestream reference condition at Mach number of 0.04 is arbitrarily chosen to normalize the aerodynamic parameters at static conditions. They include $V_\infty = 9.3\,\mathrm{m/s}$ and $\rho_\infty = 0.0158\,\mathrm{kg/m^3}$. The first grid point on the airfoil surface is placed at $y^+ \approx 1$.

The atmospheric properties for Mars, relevant to the present analysis, are summarized in Table 1.

Table 1: Flow Conditions and Properties

Variable	**Value**	**Unit**
p	655	[Pa]
T	220	[K]
ρ	0.01576	[kg/m^3]
μ	1.11E-05	[kg/m s]
R	188.9	[J/kg K]
L_{ref}	1	[m]
U_∞	9.3	[m/s]
γ	1.3	
M_∞	0.04	
Re_∞	1.32E+04	

3 Results and Discussion

3.1 Propeller D_p and CFJ Injection size effect

This section investigates the effects of propeller intensity and CFJ injection size on the flow characteristics. For this study, a propeller with a diameter of 1.75 times the chord length is positioned 1 chord length downstream in the horizontal direction and 0.59 chord lengths above the airfoil.

The impact of the propeller intensity, expressed as the pressure jump ratio (D_p), on the lift coefficient (C_L) is examined. As D_p increases, a higher jet momentum coefficient (C_μ) from the CFJ system

is required to maintain flow attachment. Figures 4 and 5 illustrate the role of C_μ in achieving flow attachment for D_p of 2%. When C_μ is set to 10, the flow detaches from the coflow surface. Increasing C_μ to 12 enhances the coflow jet energy, resulting in flow attachment with accelerated velocity from the airfoil leading edge to the coflow injection point and a 1.6 times increase in C_L.

When C_μ is increased to 12, the system maintains attached flow without separation, with a power coefficient (P_c) of 40.41. This represents a 30% reduction in P_c compared to the $C_\mu = 10$ case, where P_c is 57.5, demonstrating the importance of maintaining attached flow for improved efficiency even when C_μ is increased.

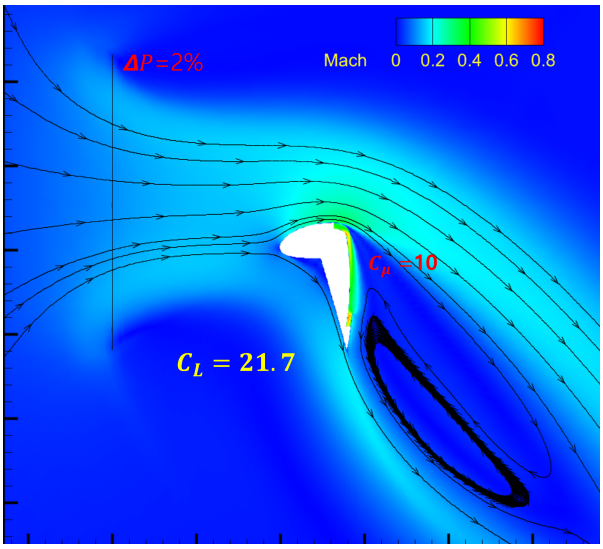

Figure 4: Mach contour with Dp 2% at C_μ 10

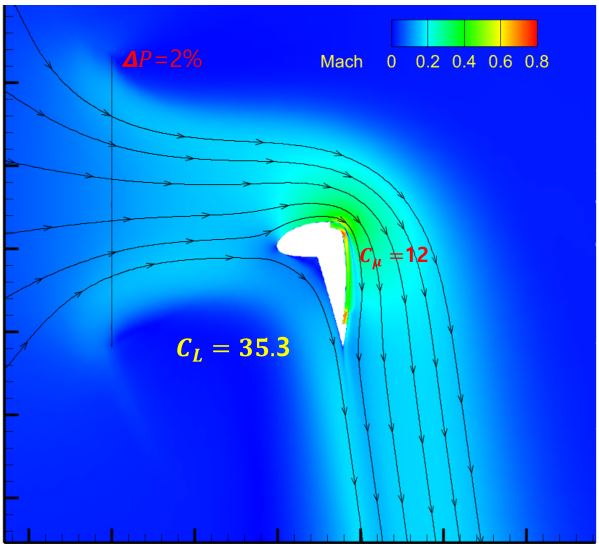

Figure 5: Mach contour with Dp 2% at C_μ 12

Figure 6 shows a highly linear relationship between D_p and C_L, demonstrating a strong correlation coefficient that validates the theoretical predictions from momentum theory. This linear dependency indicates that the propeller strength parameter serves as a primary control mechanism for lift generation in the deflected slipstream system. To achieve higher C_L values required for efficient Mars atmospheric operations, increasing D_p has the most significant impact on overall system performance, providing a direct and predictable means of lift enhancement. However, this increase must be accompanied by a corresponding and carefully calibrated increase in C_μ from the CFJ to ensure adequate flow attachment and prevent boundary layer separation, particularly at the critical deflection regions where adverse pressure gradients are most severe.

The interdependence between D_p and C_μ reveals the complexity of the flow control mechanism, where insufficient jet momentum coefficient can lead to flow separation despite adequate D_p, while excessive C_μ may result in diminishing returns due to increased power consumption. This balance becomes increasingly critical as the deflection angle β increases, since larger deflections impose stronger adverse pressure gradients that require more energetic jet injection to maintain attachment. However, increasing C_μ also raises the compressor total pressure ratio Γ, which presents significant engineering challenges in terms of micro-compressor design, efficiency, and integration within the airfoil structure. The elevated pressure ratios demand more sophisticated compression systems that can maintain high efficiency while operating at the compact scales required for airfoil integration, particularly considering the stringent weight and volume constraints inherent in Mars aircraft design.

Figure 7 examines the effect of CFJ injection size on the total pressure ratio under controlled conditions where the momentum coefficient $C_\mu = 10$ and propeller strength $D_p = 2\%$ are held constant, revealing an inverse power-law relationship that follows a -0.4 power scaling. As injection size increases, the total pressure ratio decreases proportionally, following the relationship $\Gamma \propto Inj\_size(\%C)^{-0.4}$, where $Inj\_size(\%C)$ represents the injection slot size normalized by chord length. The physical mechanism underlying this relationship stems from the reduced injection velocity required to achieve the same momentum coefficient when the slot area is increased, thereby reducing the compression work needed from the micro-compressor system. Since C_μ is proportional to the product of mass flow rate and injection velocity, maintaining constant C_μ while increasing slot area necessitates a corresponding decrease in injection velocity, which directly translates to lower total pressure ratio requirements.

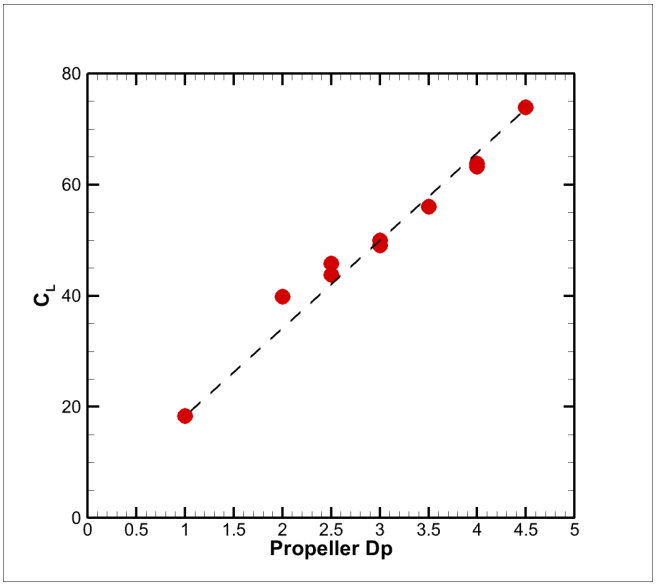

Figure 6: Lift coefficient (C_L) effect on Propeller strengh D_p

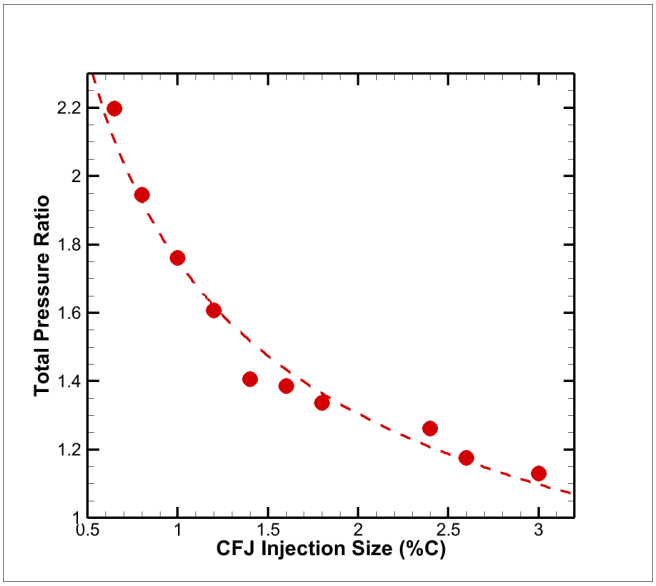

Figure 7: Total pressure ratio effect on CFJ Injection size

Table 2 presents comprehensive results for the parametric study involving injection size, suction size, propeller strength D_p, and momentum coefficient C_μ under hover conditions. The data reveals significant challenges in achieving the lift coefficients necessary for practical Mars aircraft operations. At hover, it is the static condition with freestream velocity equal to zero. The reduced dynamic pressure at zero velocity at a static condition directly impacts the lift generation capability of the airfoil system regardless of the flow control effectiveness.

Considering the lift force requirements for efficient cruise operation in the Martian atmosphere, a minimum $C_{L,\text{total}}$ of approximately 70 is required to ensure adequate aircraft performance and payload capacity. To satisfy this demanding requirement, the geometric and operational parameters are pushed to their practical limits: the injection size and suction size are required to be 3.2%C and 4.5%C, respectively, while the propeller strength D_p must reach 4.5% (8). These specifications represent a significant scaling up from conventional CFJ configurations and approach the boundaries of what is mechanically feasible within typical airfoil thickness constraints.

However, achieving these conditions presents formidable engineering challenges that extend beyond pure aerodynamic considerations. The manufacturing and integration of CFJ ducts with such large

cross-sectional areas becomes increasingly difficult, particularly when considering the structural integrity requirements and the limited internal volume available within a practical airfoil geometry. The internal ducting system must accommodate not only the enlarged injection and suction slots but also the associated micro-compressor hardware, control systems, and structural reinforcements, all while maintaining the aerodynamic shape integrity of the airfoil. Furthermore, there exists a critical operational challenge in that C_μ must reach approximately 30 to generate sufficient jet intensity for effective flow control at these high lift coefficients, which results in very high power consumption levels that may compromise the overall system efficiency and mission viability for Mars aircraft applications.

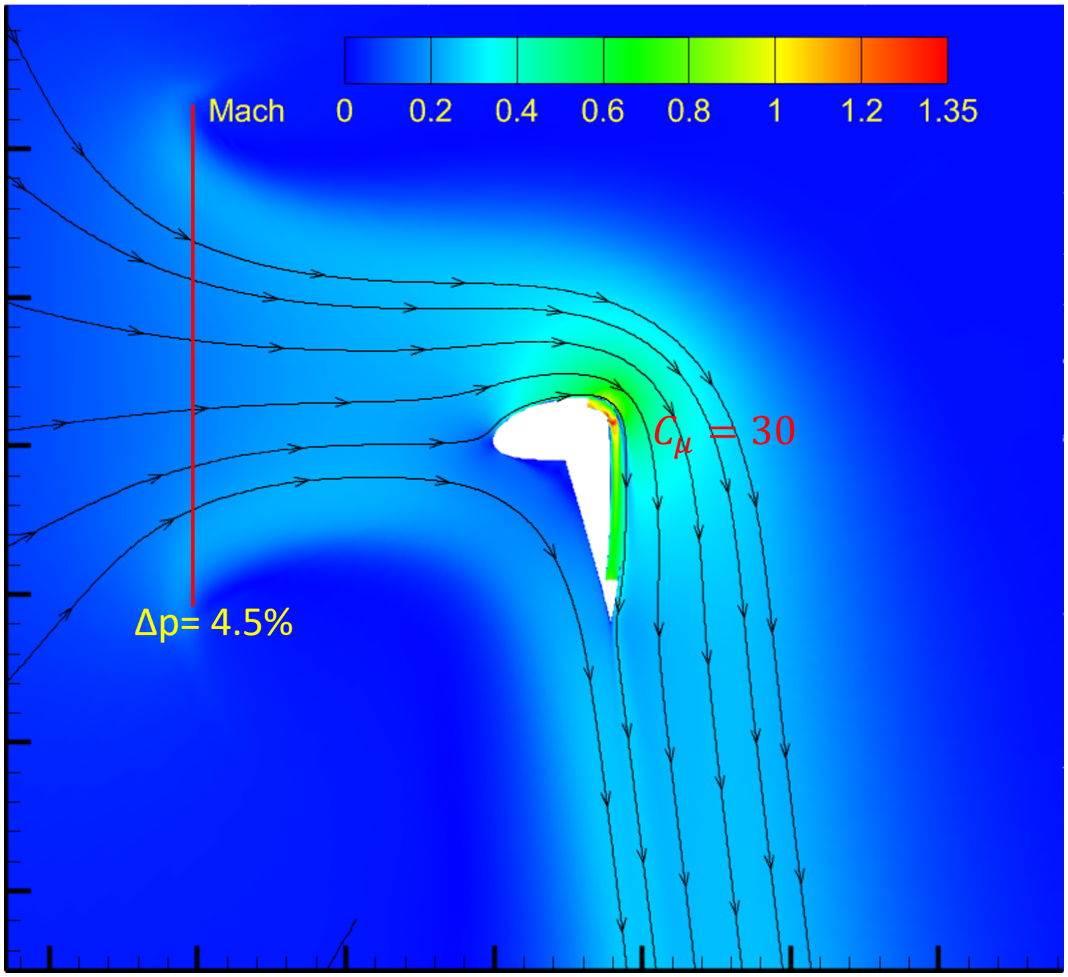

Figure 8: Mach contour of case for injection size 3.2 %C with Propeller Dp 4.5 %

Table 2: Results for Hover condition without airfoil tilting

Inj_size (%C)	Suc_size (%C)	D_p (%)	C_μ	$C_{L,\text{airfoil}}$	$C_{D,\text{airfoil}}$	$P_{c,\text{cfj}}$	Γ	$C_{L,\text{prop}}$	$C_{D,\text{prop}}$	P_p	$C_{L,\text{total}}$	$C_{D,\text{total}}$	ϵ (deg)
0.65	1.33	1.0	8	18.38	16.33	111.09	1.91	0	-13.98	19.76	18.38	2.35	82.7
0.65	1.33	2.0	10	39.83	37.02	161.90	2.20	0	-27.71	55.14	39.83	9.31	76.8
0.8	1.33	2.0	10	39.93	36.99	125.44	1.95	0	-28.32	56.97	39.93	8.66	77.8
1.0	1.7	2.0	10	36.10	33.69	126.22	1.76	0	-26.83	52.54	36.10	6.85	79.3
1.2	1.7	2.0	10	37.08	34.54	114.39	1.61	0	-26.70	52.13	37.08	7.84	78.1
1.4	2.7	2.0	10	37.89	35.16	87.06	1.41	0	-26.79	52.41	37.89	8.37	77.5
1.6	2.7	2.0	10	35.75	33.42	77.05	1.39	0	-26.70	52.13	35.75	6.72	79.3
1.8	2.7	2.0	10	37.99	34.93	82.97	1.34	0	-26.84	52.55	37.99	8.09	78.0
2.4	3.5	2.0	10	36.64	33.33	77.91	1.26	0	-26.65	52.01	36.64	6.68	79.7
2.6	2.6	2.0	10	21.69	16.41	57.50	1.18	0	-27.43	54.30	21.69	-11.02	116.9
3.0	3.0	2.0	10	25.65	20.83	45.64	1.13	0	-27.78	55.33	25.65	-6.95	105.2
2.6	2.6	2.5	20	43.74	39.82	70.98	1.16	0	-27.42	54.28	43.74	12.40	74.2
2.6	2.6	3.0	20	49.92	44.87	74.78	1.17	0	-42.61	105.13	49.92	2.26	87.4
2.6	2.6	3.0	25	49.06	44.21	87.50	1.18	0	-42.92	106.27	49.06	1.29	88.5
2.6	2.6	3.5	25	56.05	50.57	89.79	1.19	0	-50.37	135.13	56.05	0.20	89.8
2.6	2.6	4.0	25	63.26	56.94	95.24	1.20	0	-57.81	166.12	63.26	-0.87	90.8
2.6	2.6	4.0	30	63.78	57.78	100.81	1.21	0	-57.79	166.06	63.78	-0.01	90.0
3.2	4.5	4.5	30	75.68	66.70	137.63	1.23	0	-74.41	242.59	75.68	-7.71	95.8

3.2 Tilting angle θ effect

The target C_L is achieved, but the injection and suction sizes are excessively large, which not only presents significant physical challenges for CFJ duct installation within the airfoil structure, but also demands high CFJ power consumption. To address these limitations, the effect of tilting the entire system is investigated as a potential solution. The optimized injection and suction sizes of 0.6%C and 1.3%C, previously determined for cruise conditions, are employed to evaluate the impact of system tilting on hover performance. Figure 9 and Table 3 demonstrates that as the tilting angle θ increases, the flow successfully attaches to the airfoil surface with a Dp of 4.5% , and with a much lower CFJ momentum coefficient $C\mu$ of 5. This improvement in flow attachment is attributed to the reduced adverse pressure gradient distribution achieved through geometric reorientation of the airfoil relative to the propeller slipstream. The optimal configuration is obtained when $\theta = 20$, yielding a total lift coefficient $C_{L,\text{total}}$ of approximately 72, which precisely meets the target value required.

The system tilting approach provides substantial performance benefits beyond achieving the target lift coefficient. Compared to the non-tilted configuration that achieved the target C_L (injection size 3.2%C, suction size 4.5%C, $D_p = 4.5\%$, $C_\mu = 30$), while the total pressure ratio Γ of the CFJ compressor increases by 23% to 1.52, the CFJ power coefficient P_c is dramatically reduced by 65% to 48, representing a very significant improvement in energy efficiency. Furthermore, by utilizing the optimized injection and suction slot dimensions established for cruise conditions, the system eliminates the problematic duct installation challenges while maintaining effective flow control through simple flap deflection.

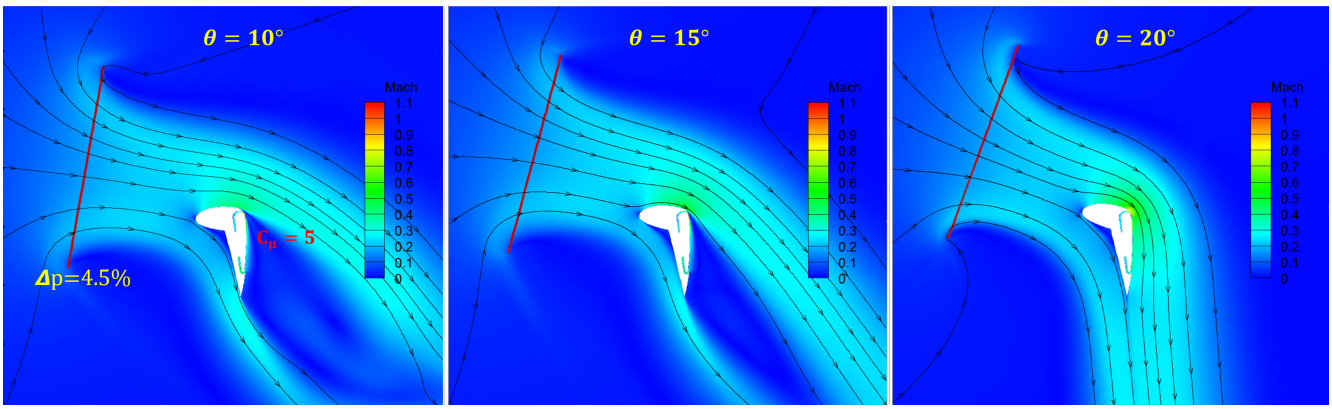

Figure 9: Mach contour according to θ at injection size=0.6%c and D_p=4.5%
(left: Case 1, middle: Case 2, right: Case 3)

Table 3: Results according to airfoil tilting angle θ

Case	θ (deg)	β (deg)	$C_{L,\text{airfoil}}$	$C_{D,\text{airfoil}}$	$P_{c,\text{cfj}}$	Γ	$C_{L,\text{prop}}$	$C_{D,\text{prop}}$	P_p	$C_{L,\text{total}}$	$C_{D,\text{total}}$	ϵ (deg)
1	10	70	28.32	33.62	80.79	1.86	11.48	-65.09	198.49	39.80	-31.47	128.3
2	15	65	33.37	35.64	77.17	1.84	16.80	-62.71	187.71	50.18	-27.07	118.3
3	20	60	47.19	65.22	47.96	1.52	24.80	-68.13	212.55	71.99	-2.91	92.3

Figure 10 and Table 4 demonstrate the effects of the CFJ momentum coefficient C_μ on aerodynamic performance. Since C_μ plays a critical role in flow attachment for CFJ airfoils, it must be optimized to minimize power consumption while maintaining adequate jet intensity. The results indicate that at $C_\mu = 2$, the flow fails to attach, resulting in significantly reduced lift generation. However, at $C_\mu = 3$ and above, successful flow attachment is achieved.

A comparative analysis between $C_\mu = 3$ and $C_\mu = 8$ reveals that while the CFJ power coefficient P_c differs by approximately a factor of 3.9, the total lift coefficient varies by only 6.5%. This suggests diminishing returns in lift enhancement beyond moderate momentum coefficient values, while power requirements continue to increase substantially.

Figure 11 presents the pressure coefficient (C_p) distribution, clearly illustrating the overall lower pressure distribution at $C_\mu = 2$ where flow separation occurs. The C_p distributions for $C_\mu = 5$ and $C_\mu = 8$ exhibit nearly identical characteristics, with only minimal differences observed in the maximum C_p values near the CFJ injection location. Correspondingly, the lift coefficient difference between these two cases is merely 2%, indicating that the flow attachment and circulation enhancement reach an optimal plateau beyond $C_\mu = 5$.

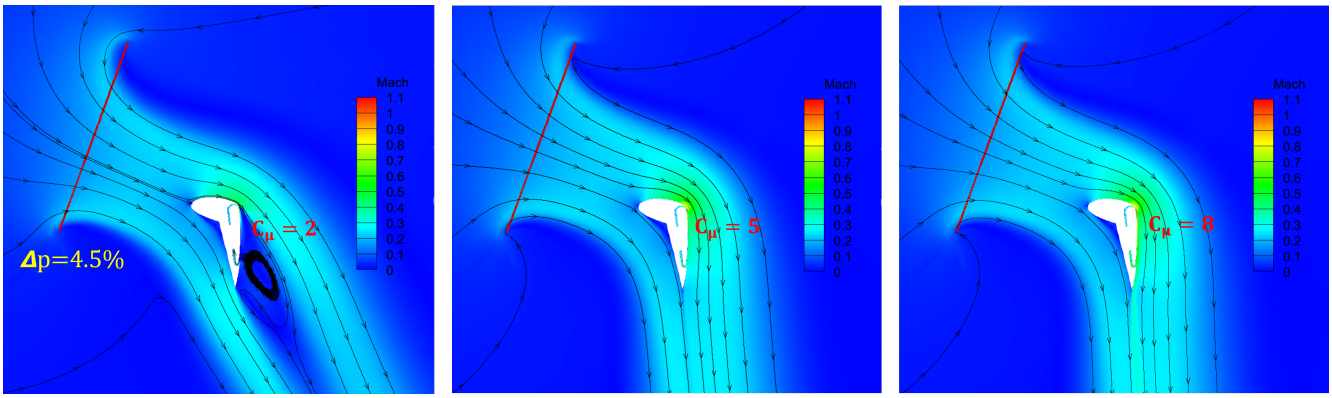

Figure 10: Mach contour according to C_μ at θ=20 (left: Case 1, middle: Case 3, right: Case 4)

Table 4: Results according to C_μ at θ=20

Case	C_μ	$C_{L,\text{airfoil}}$	$C_{D,\text{airfoil}}$	$P_{c,\text{cfj}}$	Γ	$C_{L,\text{prop}}$	$C_{D,\text{prop}}$	P_p	$C_{L,\text{total}}$	$C_{D,\text{total}}$	ϵ (deg)
1	2	26.97	39.71	25.10	1.38	24.83	-68.22	212.96	51.80	-28.50	118.8
2	3	43.37	57.41	26.57	1.35	24.83	-68.23	213.00	68.20	-10.82	99.0
3	5	47.19	65.22	47.96	1.52	24.80	-68.13	212.55	71.99	-2.91	92.3
4	8	48.15	67.48	104.03	1.90	24.79	-68.12	212.52	72.94	-0.65	90.5

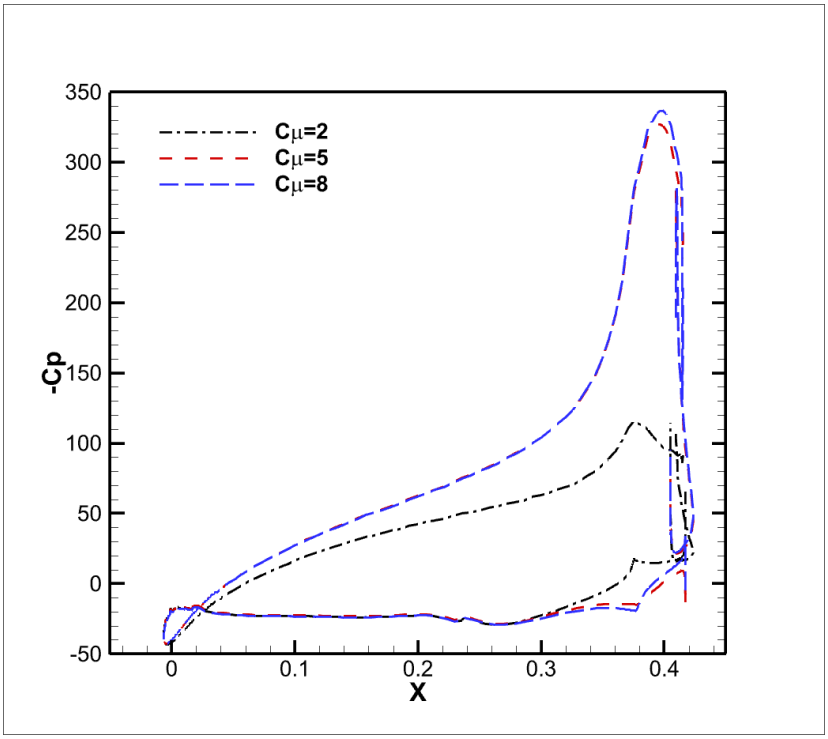

Figure 11: C_p distribution according to C_μ at θ=20

4 Conclusion

This paper presents a numerical investigation of deflected slipstream hover performance using Flapped CoFlow Jet (FCFJ) airfoils designed for low Reynolds number operations in Martian atmospheric conditions.

The parametric study reveals a highly linear relationship between propeller strength D_p and total lift coefficient $C_{L,\text{total}}$, validating theoretical predictions from momentum theory. The CFJ injection size exhibits an inverse power-law relationship with total pressure ratio, following $\Gamma \propto \text{Inj\_size}(\%C)^{-0.4}$, providing valuable design guidelines for micro-compressor integration. However, achieving the target lift coefficient of approximately 72 required for efficient Mars operations initially demanded excessively large injection and suction slot sizes (3.2%C and 4.5%C respectively) and very large CFJ momentum coefficients $C_\mu = 30$, presenting significant manufacturing and power consumption challenges.

To address these limitations, system tilting is investigated as an optimization strategy. The optimal configuration is achieved at a tilting angle $\theta = 20$ with a flap deflection angle $\beta = 60$, successfully achieving the target $C_{L,\text{total}}$ of 72 while utilizing practical injection and suction slot dimensions of 0.6%C and 1.3%C respectively. This configuration demonstrates remarkable efficiency improvements, reducing CFJ power coefficient P_c by 65% compared to the non-tilted baseline while maintaining flow attachment with $C_\mu = 5$.

The momentum coefficient analysis reveals that flow attachment is achieved at $C_\mu \geq 3$, with diminishing returns observed beyond $C_\mu = 5$. While increasing C_μ from 3 to 8 results in a 3.9-fold increase in power consumption, the corresponding lift enhancement is only 6.5%, emphasizing the importance of optimal CFJ parameter selection for energy-efficient operations.

Overall, the deflected slipstream FCFJ system demonstrates the capability to achieve the demanding hover lift requirements for Mars aircraft while maintaining reasonable power consumption and practical geometric constraints. The system tilting approach provides a viable solution for overcoming the inherent challenges of low Reynolds number hover operations, laying an important foundation for developing efficient VTOL aircraft capable of runway-independent operations in the thin Martian atmosphere.

5 Acknowledgment

The teaching assistantship support from the University of Miami is also acknowledged.

Disclosure: The University of Miami and Dr. Gecheng Zha may receive royalties for future commercialization of the intellectual property used in this study. The University of Miami is also equity owner in CoFlow Jet, LLC, licensee of the intellectual property used in this study.

References

[1] K. Fujita, R. Luong, H. Nagai, and K. Asai, "Conceptual design of mars airplane," *Trans. JSASS Aerospace Tech. Japan*, vol. 10, no. ists28, pp. 5–10, 2012.

[2] Y. Ren and G. Zha, "Simulation of 2d coflow jet deflected slipstream vtol transition transient flows," in *10th Annual Electric VTOL Symposium*, (Mesa, AZ), January 2023.

[3] Y. Ren and G. Zha, "2d fluid-body interaction simulation of coflow jet deflected slipstream vtol transition flight," in *AIAA AVIATION FORUM AND ASCEND 2024, AIAA 2024-4419*, (Las Vegas, Nevada), 29 July - 2 August 2024.

[4] G. Zha, "Feasibility study of deflected slipstream airfoil for vtol hover enabled by coflow jet," in *AIAA Aviation Forum 2023, AIAA 2023-4279*, (San Diego, CA), June 2023.

[5] G.-C. Zha and D. C. Paxton, "A novel flow control method for airfoil performance enhancement using co-flow jet," in *Applications of Circulation Control Technologies* (R. D. Joslin and G. Jones, eds.), vol. 214 of *Progress in Astronautics and Aeronautics*, ch. 10, pp. 293–314, AIAA Book Series, 2006.

[6] G.-C. Zha, W. Gao, and C. Paxton, "Jet effects on co-flow jet airfoil performance," *AIAA Journal*, vol. 45, no. 6, pp. 1222–1231, 2007.

[7] G.-C. Zha, C. Paxton, A. Conley, A. Wells, and B. Carroll, "Effect of injection slot size on the performance of coflow jet airfoil," *AIAA Journal of Aircraft*, vol. 43, no. 4, 2006.

[8] G.-C. Zha, B. Carroll, C. Paxton, A. Conley, and A. Wells, "High performance airfoil with co-flow jet flow control," *AIAA Journal*, vol. 45, no. 8, 2007.

[9] B.-Y. Wang, B. Haddoukessouni, J. Levy, and G.-C. Zha, "Numerical investigations of injection slot size effect on the performance of co-flow jet airfoil," *Journal of Aircraft*, vol. 45, no. 6, pp. 2084–2091, 2008.

[10] B. P. E. Dano, D. Kirk, and G.-C. Zha, "Experimental investigation of jet mixing mechanism of co-flow jet airfoil," in *5th AIAA Flow Control Conference, AIAA 2010-4421*, (Chicago, IL), June–July 2010.

[11] B. P. E. Dano, G.-C. Zha, and M. Castillo, "Experimental study of co-flow jet airfoil performance enhancement using micro discreet jets," in *49th AIAA Aerospace Sciences Meeting, AIAA 2011-941*, (Orlando, FL), January 2011.

[12] A. Lefebvre, B. Dano, W. Bartow, M. Fronzo, and G. Zha, "Performance and energy expenditure of coflow jet airfoil with variation of mach number," *Journal of Aircraft*, vol. 53, no. 6, pp. 1757–1767, 2016.

[13] A. Lefebvre and G.-C. Zha, "Numerical simulation of pitching airfoil performance enhancement using co-flow jet flow control," in *31st AIAA Applied Aerodynamics Conference, AIAA 2013-2517*, June 2013.

[14] A. Lefebvre and G.-C. Zha, "Co-flow jet airfoil trade study part i : Energy consumption and aerodynamic performance," in *AIAA Aviation, AIAA 2014-2682*, June 2014.

[15] A. Lefebvre and G.-C. Zha, "Co-flow jet airfoil trade study part ii : Moment and drag," in *AIAA Aviation, AIAA 2014-2683*, June 2014.

[16] Y. Yang and G. Zha, "Super-lift coefficient of active flow control airfoil: What is the limit?," in *55th AIAA Aerospace Science Meeting, AIAA 2017-1693*, (Grapevine, Texas), January 2017.

[17] G. Zha, Y. Yang, Y. Ren, and B. McBreen, "Super-lift and thrusting airfoil of coflow jet actuated by micro-compressors," in *AIAA AVIATION Forum 2018, Flow Control Conference, AIAA 2018-3061*, June 2018.

[18] A. Lefebvre and G.-C. Zha, "Trade study of 3d co-flow jet wing for cruise performance," in *AIAA SCITECH2016, AIAA Aerospace Science Meeting, AIAA 2016-0570*, (San Diego, CA), January 2016.

[19] K. Xu and G. Zha, "High control authority 3d aircraft control surfaces using co-flow jet," *AIAA Journal of Aircraft, Vol 58, Issue 1, p72-84*, 2021.

[20] K. Xu, Y. Ren, and G. Zha, "Numerical analysis of energy expenditure for co-flow wall jet separation control," *AIAA Journal*, 2022. published online: 11 Jan 2022, doi.org/10.2514/1.J061015.

[21] Y. Wang and G. Zha, "Study of mach number effect for 2d co-flow jet airfoil at cruise conditions," in *AIAA Aviation 2019 Forum, AIAA 2019-3169*, (Dallas, Texas), June 2019.

[22] Y. Wang and G. Zha, "Study of mach number effect for 3d co-flow jet wings at cruise conditions," in *AIAA SciTech Forum, AIAA 2020-0045*, (Orlando, FL), January 2020.

[23] Y. Ren and G. Zha, "Performance enhancement by tandem wings interaction of coflow jet aircraft," in *AIAA SciTech Forum, AIAA 2020-1823*, (VIRTUAL EVENT), January 2021.

[24] Y. Wang, Y. Yang, and G. Zha, "Study of super-lift coefficient of co-flow jet airfoil and its power consumption," in *AIAA Aviation 2019 Forum, AIAA 2020-3652*, (Dallas, Texas), June 2019.

[25] J. Jeon, Y. Ren, and G. Zha, "Toward ultra-high cruise lift coefficient using flapped coflow jet airfoil," in *AIAA SciTech Forum, AIAA 2023-1008*, January 2023.

[26] J. Jeon, B. McBreen, Y. Ren, and G. Zha, "Study of 3d flapped coflow jet wings for ultra-high cruise lift coefficient," in *AIAA Aviation Forum, AIAA 2023-4436*, June 2023.

[27] J. Jeon, Y. Ren, and G. Zha, "Flapped coflow jet airfoil for high lift cruise at low reynolds number in martian atmosphere," in *AIAA SciTech Forum, AIAA 2024-1727*, January 2024.

[28] J. Jeon, Y. Ren, and G. Zha, "Flapped coflow jet wing for high lift cruise in the martian atmosphere," in *AIAA Aviation Forum, AIAA 2024-3589*, July–August 2024.

[29] K. Xu, Y. Ren, and G. Zha, "Separation control by co-flow wall jet," in *AIAA AVIATION Forum, AIAA 2021-2946*, August 2021.

[30] K. Xu and G. Zha, "Design of high specific speed mixed flow micro-compressor for co-flow jet actuators," in *ASME IGTI Turbo Expo 2019*, (Phoenix, Arizona, USA), pp. GT–2019–90980, June 2019.

[31] P. A. Barrios, Y. Ren, and G. Zha, "Simulation of 3d co-flow jet airfoil control with micro-compressor actuator at high angles of attack," in *AIAA Aviation Forum 2023, AIAA 2023-4208*, (San Diego, CA), June 2023.

[32] P. R. Spalart and S. R. Allmaras, "A one-equation turbulence model for aerodynamic flows," in *30th Aerospace Sciences Meeting and Exhibit*, (Reno, NV, USA), pp. https://doi.org/10.2514/6.1992–439, 1992.

[33] Y.-Q. Shen and G.-C. Zha, "Large eddy simulation using a new set of sixth order schemes for compressible viscous terms," *Journal of Computational Physics*, vol. 229, pp. 8296–8312, 2010.

[34] G. Zha, Y. Shen, and B. Wang, "An improved low diffusion e-cusp upwind scheme," *Journal of Computer and Fluids*, vol. 48, pp. 214–220, September 2011.

[35] Y.-Q. Shen and G.-Z. Zha, "Generalized finite compact difference scheme for shock/complex flowfield interaction," *Journal of Computational Physics*, 2011. doi:10.1016/j.jcp.2011.01.039.

[36] Y.-Q. Shen, G.-C. Zha, and B.-Y. Wang, "Improvement of stability and accuracy of implicit weno scheme," *AIAA Journal*, vol. 47, no. 2, pp. 331–344, 2009.

[37] Y.-Q. Shen, G.-C. Zha, and X.-Y. Chen, "High order conservative differencing for viscous terms and the application to vortex-induced vibration flows," *Journal of Computational Physics*, vol. 228, no. 2, pp. 8283–8300, 2009.

[38] Y.-Q. Shen and G.-C. Zha, "Improvement of the weno scheme smoothness estimator," *International Journal for Numerical Methods in Fluids*, 2009. DOI:10.1002/fld.2186.

[39] G.-C. Zha and E. Bilgen, "Numerical study of three-dimensional transonic flows using unfactored upwind-relaxation sweeping algorithm," *Journal of Computational Physics*, vol. 125, pp. 425–433, 1996.

[40] B.-Y. Wang and G.-C. Zha, "A general sub-domain boundary mapping procedure for structured grid cfd parallel computation," *AIAA Journal of Aerospace Computing, Information, and Communication*, vol. 5, no. 11, pp. 2084–2091, 2008.

[41] Y.-Q. Shen, G.-C. Zha, and B.-Y. Wang, "Improvement of stability and accuracy of implicit weno scheme," *AIAA Journal*, vol. 47, no. 11, pp. 331–344, 2009.